Composites: Part A 177 (2024) 107894

Contents lists available at ScienceDirect

Composites Part A

journal homepage: www.elsevier.com/locate/compositesa

Resistance-welded thermoset composites: A Bayesian approach to process optimisation for improved fracture toughness

Thomas Maierhofer [a,*], Evripides G. Loukaides [b], Craig Carr [c], Chiara Bisagni [d], Richard Butler [a]

[a] Centre for Integrated Materials, Processes & Structures (IMPS), Department of Mechanical Engineering, University of Bath, Claverton Down, Bath, BA2 7AY, United Kingdom

[b] Centre for Digital, Manufacturing & Design (dMaDe), Department of Mechanical Engineering, University of Bath, Claverton Down, Bath, BA2 7AY, United Kingdom

[c] GKN Aerospace, Global Technology Centre, Taurus Rd, Bristol, BS34 6FB, United Kingdom

[d] Department of Aerospace Science and Technology, Politecnico di Milano, Via La Masa 34, Milan, 20156, Italy

ARTICLE INFO

Keywords:
A. Thermosetting resin
B. Fracture toughness
C. Statistical properties/methods
E. Joints/joining
E. Fusion bonding

ABSTRACT

Joining thermoset composites via resistance welding offers a novel highly efficient assembly method for next-generation aerospace structures. Resistance-welded joints combine the benefits of bonding with the capacity for high-volume manufacturing rates and eliminate the need for complex surface preparation. The influence of key welding parameters on the joint performance is investigated by assessing the Mode I fracture toughness. Double Cantilever Beam specimens with different welding parameter combinations are manufactured, tested and compared with each other. Thermoset laminates are made weldable by co-curing a chemically compatible thermoplastic film with an uncured thermoset laminate. A Bayesian approach is used to study the correlation between processing parameters and to select parameters yielding high performance by training a Gaussian process emulator. Observed Mode I fracture toughness values are comparable to high-performance thermoplastic composites. This is equivalent to an improvement of approximately 290% in Mode I fracture toughness when compared to a co-cured thermoset joint.

1. Introduction

Joining of composite aerospace structures remains challenging and novel, advanced and more efficient joining methods are required for the next generation of aerospace structures. For increased application, these joining methods need to (i) offer improved structural efficiency, (ii) ease repair and disassembly of structures, (iii) reduce the complexity of assembly, and, most importantly, (iv) meet the stringent requirements for certification [1,2]. Furthermore, joining costs significantly contribute to the overall cost of composite structures, therefore more cost-effective methods are required [3].

Current joining methods for thermoset composite aerospace components include mechanical fastening and adhesive bonding [4]. Both methods have several advantages and disadvantages [1]. Mechanical fasteners require fastener holes, thus breaking fibre continuity and creating stress concentrations [5,6]. To reduce the effect of stress concentrations often additional plies are added locally, increasing the weight and reducing the efficiency of the components [7]. Thermoset adhesive bonding offers improved load distribution across the entire joint surface and thus large stress concentrations are avoided [8]. Nonetheless, adhesive bonding is labour-intensive, requires extensive surface preparation and long curing times [6,7]. Furthermore, adhesive bonding is not readily certifiable for primary aerospace structures [1]. Amongst other factors, certification of adhesively bonded joints is limited by their dependency on extensive surface preparation, curing cycle conditions and the absence of non-destructive testing methods that allow to fully assess the quality of a joint [9].

Fusion bonding (welding) is a novel joining method that offers numerous advantages over traditional joining methods. The most promising technologies are resistance, ultrasonic and induction welding [10]. Welding is already successfully applied for joining thermoplastic composite components. Parts are joined together by locally melting the interface via the application of heat and pressure [11]. It is a highly efficient method that (i) eliminates the need for complex surface preparations, (ii) offers much shorter cycle times, (iii) can more readily be reprocessed and (iv) produces high-performance joints with equivalent or improved performance when compared to adhesively bonded and mechanically fastened joints [1,4,11]. However, especially for larger components thermoset composites remain very attractive, due to their cost advantages when compared to thermoplastic composites [10].

* Corresponding author.
E-mail address: tam48@bath.ac.uk (T. Maierhofer).

https://doi.org/10.1016/j.compositesa.2023.107894
Received 2 September 2023; Received in revised form 12 October 2023; Accepted 9 November 2023
Available online 18 November 2023

Unlike thermoplastic composites, thermoset composites cannot readily be remelted and thus welded. One method of making a thermoset composite weldable is by co-curing a thermoplastic film with the uncured thermoset composite, thus creating a thermoplastic-rich surface layer [6,12]. Recent studies performed by Villegas et al. [10] and Brauner et al. [1] have shown that for chemically compatible thermosets and thermoplastics a strong bond, relying on a reaction-induced gradient interphase is formed during cure [1]. These studies primarily focused on the applicability of fusion bonding for thermoset composites by studying the lap shear strength of hybrid thermoplastic to thermoset composite and thermoset to thermoset composite joints respectively.

Resistance welding is a particularly well-established, simple process with low equipment cost and is already successfully applied in series production of secondary thermoplastic composite aerospace structures [13,14]. Brauner et al. [1] and Zweifel et al. [12] have shown that resistance welding can be used for joining thermoset composites, via a thermoplastic-rich surface layer. By using a design of experiments approach and single-lap shear coupons, approximate processing windows and lap shear strengths comparable to high-performance thermoset adhesive bonded joints were achieved [1]. Although single-lap shear tests are easy to perform and are thus a very popular method to assess adhesive properties, these tests come with several challenges. Single-lap shear tests are subject to complex loading conditions that result in uneven shear stresses, load path eccentricity and deformation in the joint interface. Thus, bending and normal forces at the joint interface occur. As a result, for composite components failure is usually driven by delamination within the adherents which rarely allows for assessment of the actual joint strength [15].

This study aims to investigate the effects of key welding parameters on the performance of aerospace-grade resistance-welded thermoset composite joints. Welding is performed using an improved process control method, adjusting the welding power based on the interface temperature and by defining the maximum permissible heating rate. The Mode I fracture toughness performance of varying manufacturing parameter combinations is assessed using Double Cantilever Beam (DCB) specimens. Mode I fracture toughness is commonly the most critical fracture mode and a key mechanical property of a composite joint [16]. In contrast to single-lap shear tests, DCB specimens are not subject to complex loading conditions and thus it is believed that the true performance of a joint can more readily be determined. A Gaussian process emulator is trained using empirical data, to study the correlation between processing parameters and identify processing windows yielding high-performance joints. Traditional regression methods rely on fitting training data to a predefined analytical function and thus have limited flexibility. In contrast, the Gaussian process approach is a nonparametric Bayesian method and is thus much more flexible [17].

2. Experimental procedure

2.1. Materials and manufacturing

Thermoset laminates used consist of 14-plies of unidirectional HexPly®IM7/8552 (CF/epoxy), with a ply thickness of 0.125 mm and a single layer of 0.25 mm thick polyetherimide (PEI) film (grade ULTEM 1000). The PEI film creates a thermoplastic-rich weldable surface layer, referred to as the coupling layer. The thickness of the PEI film was chosen based on a study performed by Tsiangou et al. [5] on the effect of varying the coupling layer thickness on the performance of ultrasonically-welded CF/epoxy to CF/PEEK (polyetheretherketone) laminates. It was demonstrated that a coupling layer thickness of 250 μm allows for a comparable wide range of processing parameters to be used. Decreasing the thickness to a very thin layer of 60 μm resulted in a decrease in mechanical performance as well as signs of thermal degradation occurred before a fully welded joint was achieved [5]. Amorphous polymers such as PEI are prone to absorb moisture, which can lead to the formation of voids during the processing phase and thus adversely affect the mechanical performance of the joint post-welding [18]. Therefore, to minimise the moisture content the PEI film was dried at 120 °C for 5 h using an air circulating oven prior to co-curing. Using the manufacturer's recommended autoclave cycle, maintaining a maximum temperature of 180 °C and 0.7 MPa pressure for 120 min, the PEI film was co-cured with the uncured thermoset laminate. The average cured total laminate thickness was 2.0 mm.

Commonly used epoxy resin systems and PEI are chemically compatible and show solubility prior to co-curing [19]. Initial solubility between the thermoset matrix and the thermoplastic film favours the occurrence of mutual diffusion mechanisms. After establishing contact between the thermoplastic and the thermoset, swelling of the thermoplastic occurs due to the diffusion of thermoset monomers into the thermoplastic. Components of the epoxy resin then partially dissolve polymer chains of the thermoplastic allowing for interdiffusion between both materials. During the initial phase of the thermoset cure cycle the diffusion rate is high due to the apparent low molecular weight [20]. Once the gelation point of the thermoset matrix is reached, further interdiffusion is restricted and phase separation occurs [1,19]. A heterogeneous morphology with a thermoset- and a thermoplastic-rich phase, with strong micromechanical interlocking occurs. Thus a strong bond based on a reaction-induced gradient interphase forms between the PEI film and the CF/epoxy laminate as a result of their initial solubility and chemical compatibility [1]. Brauner et al. [1] and Zweifel et al. [20] have extensively studied the diffusion and dissolution behaviour of co-cured thermoplastics with thermoset epoxy matrix systems. Zweifel et al. [20] have investigated novel in-situ characterisation methods to study the reaction–diffusion process during co-curing of a PEI film with an epoxy-amine thermoset allowing to investigate in detail the initial interphase formation phase of PEI and an epoxy system.

To identify the thickness of this interphase, cross-section specimens of welded samples were created for optical microscopy analysis. To create a visible contrast between PEI and the epoxy matrix, PEI was partially dissolved, by etching the samples using N-Methyl-2-pyrrolidone (NMP) [19]. Therefore 1 ml of NMP was dripped onto the samples, immediately followed by rinsing them with isopropanol and distilled water, and drying them using compressed air [19]. A cross-section microscopy image of the welded joint and the interphase post NMP etching are shown in Figs. 1(a) and 1(b) respectively. The interphase formed during the co-curing process is shown by the dark grey area between the CF/epoxy laminate and the PEI film. Both the PEI film and the matrix of the CF/epoxy laminate are represented by lighter shades of grey. Optical microscopy of the samples revealed that an interphase of approximately 8–15 μm formed. Furthermore, it can be seen in Fig. 1(b) that during the co-curing process, individual fibres become partially immersed in the thermoplastic surface layer, which was also observed by Brauner et al. [1].

Resistance welding requires the use of a heating element (HE) that allows local heating of the joint interface. Post-welding the HE remains within the joint interface [21]. For this study, a metal mesh was used for the conductor of the HE. The mesh size was chosen based on the outcomes of a study on the size effects of metal meshes in resistance-welded thermoplastic composite joints performed by Dubé et al. [22]. The key parameters for metallic meshes are the open gap width and wire thickness. Thick wire meshes were found to have similar effects to inclusion defects, therefore reducing the performance, whereas increasing the open gap width is expected to increase the performance. However, the open gaps width is limited as a too large ratio of open gap size vs. wire thickness may result in non-uniform heating [22]. Therefore, a plain weave stainless steel mesh with a wire thickness of 40 μm and an open gaps width of 87 μm was used as the conductor. Current leakage is one of the biggest challenges in resistance welding and is a result of contact between the conductor and the conductive carbon fibres (CFs) of the bulk material [13,23,24]. Methods to prevent current leakage include, (i) the application of a non-conductive coating

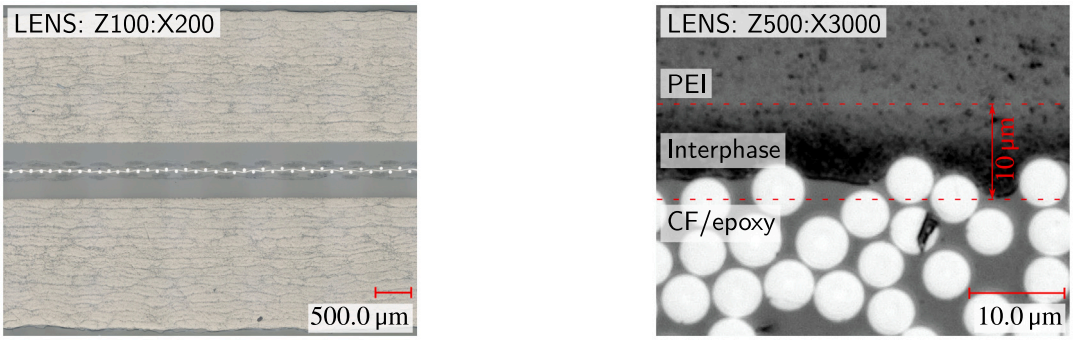

(a) Untreated sample. (b) Interphase focused view of NMP treated sample.

Fig. 1. Optical microscopy images of cross-section samples.

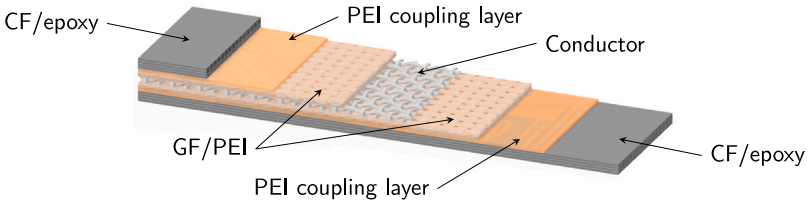

Fig. 2. Schematic of a resistance-welded joint.

on the conductor [23,25], (ii) the addition of neat resin films [24,26] and adding layers of glass fibre (GF) fabric [13,14]. In this study, the conductor of the HE was electrically isolated by applying a ply of 4-harness satin weave glass fibre PEI prepreg (Toray TC1000/EC5) on either side of the conductor. The individual layers of the HE were not pre-consolidated prior to welding. Fig. 2 illustrates the individual layers of a resistance-welded joint.

2.2. Resistance welding

The key components required for resistance welding are (i) an electrical power supply unit, (ii) a pressure application tool and (iii) clamp connectors, connecting the power supply unit with the HE's conductor [2]. Current flow is applied to the HE's conductor thus generating heat at the joint interface following Joule's law. Once the temperature exceeds the glass transition temperature for amorphous polymers or the melting point for semi-crystalline polymers, the thermoplastic coupling layer and matrix of the HE melt. Pressure is applied throughout the welding process to establish intimate contact at the interface and promote molecular diffusion. Following current application, the weld is allowed to cool whilst pressure remains applied until the interface is fully reconsolidated [24]. An illustration of the key components of a resistance welding rig is shown in Fig. 3.

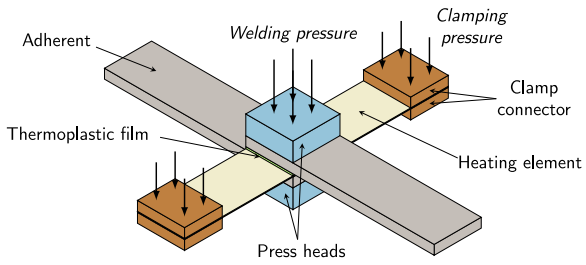

Fig. 3. Schematic of a typical resistance welding process.

Resistance welding was performed using an in-house developed resistance welding rig. The rig consists of a 10 kW DC power supply unit with a maximum output of 200 V and 140 A, a pneumatic press adjustable for different sample configurations, a pneumatic clamping system to connect the conductor of the HE with the power supply unit and a computer control and data acquisition system. The required welding pressure is applied via an aluminium press head and aluminium base plate which act as heatsinks and cool the outer surfaces of the thermoset laminates during the welding process. An in-house developed proportional integral derivative (PID) controller based software, adjusting the power output based on in-situ interface temperature monitoring and specified heating rates was used for process control. The resistance welding rig is shown in Fig. 4.

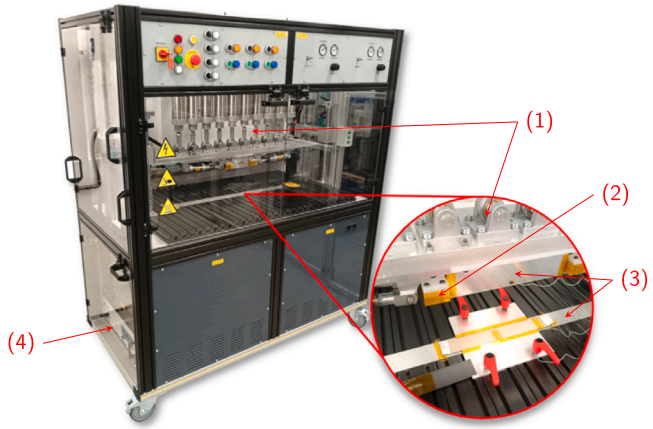

Fig. 4. Custom-made resistance welding rig at the University of Bath. Arrows indicate the key components; (1) the pneumatic press, (2) the clamp connectors, (3) the press heads/heatsinks and (4) the DC power supply unit.

The laminates were cut into coupons with a width of 43 mm and a length of 250 mm and 325 mm for the top and bottom adherents. Two K-type thermocouples were placed at the joint interface between the PEI coupling layer and the GF/PEI layer, central in the widthwise direction and lengthwise outside of the region DCB specimens were cut from. Prior to welding, a 13 µm thick polyimide film was placed between the

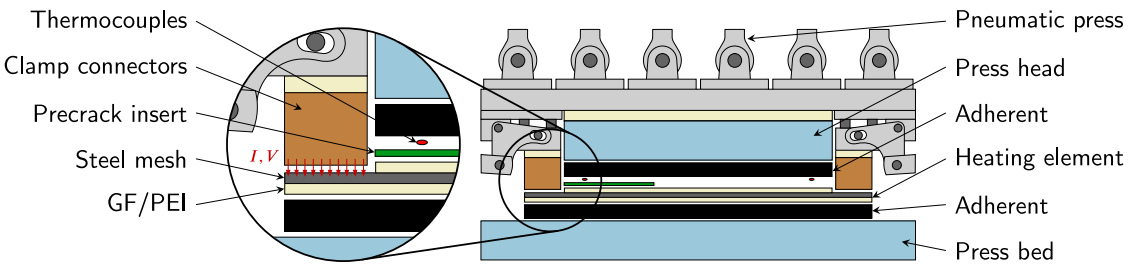

Fig. 5. Schematic of the welding process outlining the location of the individual components of the sample, the pressure application tool and connection of the heating element to the power supply unit during the welding process.

CF/epoxy laminate and the GF/PEI insulator to initiate a precrack at the joint interface.

Fig. 5 illustrates the placement of the adherents and heating element during the welding process, the location of the thermocouples, the pneumatic pressure application tool and connection of the heating element to the power supply unit via the clamp connectors.

Cut adherents and the GF/PEI layers were dried at 120 °C for 5 h, ultimately prior to welding to minimise their moisture content. A constant welding pressure was applied before current application and was applied until the temperature of the samples was well below the glass transition temperature of PEI post welding. The entire processing cycle consists of a pre-heat phase, followed by heating the interface to the target welding temperature, maintaining it for a set amount of time and uncontrolled cooling. One of the main challenges of welding thermoset composites is to avoid thermal degradation of the thermoset matrix due to the required high processing temperatures of aerospace-grade thermoplastics, such as PEI [10,27]. To minimise the risk of thermal degradation, short welding cycles and lower welding temperatures are preferred [27].

The quality and performance of a resistance-welded joint primarily depend on three processing parameters: (i) temperature (directly linked with specific power), (ii) welding pressure and (iii) duration of constant heat application. Short and low-temperature welding may result in weak or insufficiently welded joints whereas long and high-temperature welding increases the risk of thermal degradation of the thermoset matrix [12]. Welding pressure is required to prevent deconsolidation and to remove trapped air from the joint interface. However, high pressures may yield excessive squeeze flow of the molten thermoplastic [22]. The effect of varying processing parameters on the joint's mechanical performance was studied by testing different parameter combinations. The studied parameter ranges are outlined in Table 1.

Table 1
Investigated key welding parameter ranges.

Parameter	Minimum	Maximum
Time [s]	10	90
Temperature [°C]	250	350
Pressure [MPa]	0.7	1.5

2.3. Testing and fracture toughness analysis

The Mode I fracture toughness was studied according to the ASTM D5528 standard [28]. One DCB specimen per welding parameter configuration was cut from the centre of the welded samples. Welded samples were cut to 21 mm in width and 160 mm in length with a precrack insert length of 63 mm (equivalent to a precrack length of approx. 50 mm). The precise location of the precrack insert for each specimen was determined using optical microscopy. Fig. 6 illustrates the specimen design configuration.

The side faces of the samples were spray-painted using white acrylic paint to enhance the contrast between the crack and the sample. An adapted version of the side clamped beam loading blocks developed by Renart et al. [29] was used for load introduction. Specimens were tested using an Instron 50 kN universal testing machine, with a load rate of 1 mm/min in standard laboratory conditions. Crosshead displacement and force of the testing rig were recorded. Crack length gauges with an accuracy of ±0.5 mm were bonded to the specimens' side faces and the crack extension was recorded using a 4k camera. All specimens were loaded (initial loading) to grow the crack from the tip of the precrack insert to a length of approximately 5 mm. Specimens were then unloaded, the position of the new crack front was recorded and finally reloaded until a crack length of 50 mm was reached.

Calculation of the Mode I fracture toughness (G_{IC}) values was performed according to ASTM D5528, using the modified beam theory method, as it resulted in the most conservative fracture toughness for the majority of samples tested [30]. The G_{IC} was calculated using Eq. (1).

$$G_{IC} = \frac{3P\delta}{2b\,(a + |\Delta|)} \left(\frac{D}{S}\right), \tag{1}$$

where P is the measured load, δ the measured end displacement, b the specimen width and a the crack length. The modified beam theory accounts for the additional rotation at the crack front by increasing the crack length a by $|\Delta|$. The effective disbond extension $|\Delta|$ is determined via the least squares fit of the cube root of the compliance (the ratio of load point displacement and force) vs. the crack length. Large displacement effects and stiffening of the specimens due to the loading blocks are accounted for via D and S respectively [28].

For each parameter configuration, only one specimen was tested. Based on previous studies on the Mode I fracture toughness of resistance-welded hybrid and thermoplastic joints performed by the authors [30] and Araújo et al. [31], standard deviations between 10%–15% are expected. Therefore, to increase the confidence in results associated with each set of welding parameters, testing multiple samples per configuration would be necessary. However, for this study, it was decided to focus on the exploration of the parameter space rather than finding optimum values and their associated uncertainty (exploitation). The uncertainty at each point in the parameter space is accounted for by including noise in the Gaussian process emulator, as described in Section 3. Noise levels were chosen such that the minimum standard deviation is approximately 12%.

3. Gaussian process emulator for performance prediction

Identifying correlations between processing parameters and defining processing parameter windows is challenging and would require extensive testing of different parameter combinations in the design space. A stochastic approach offers an efficient method to significantly reduce the number of experiments required. Therefore, a 3-dimensional multivariate Gaussian process (GP) emulator was trained using empirical data. The three main processing parameters (i) temperature, (ii) pressure and (iii) welding time are components of the vector x and $f(x)$ is the associated Mode I fracture toughness of the joint.

Gaussian processes are a nonparametric Bayesian method. They are a collection of infinite-dimensional Gaussian distributions and are applicable even to small sets of data [32]. Any finite subset of these has

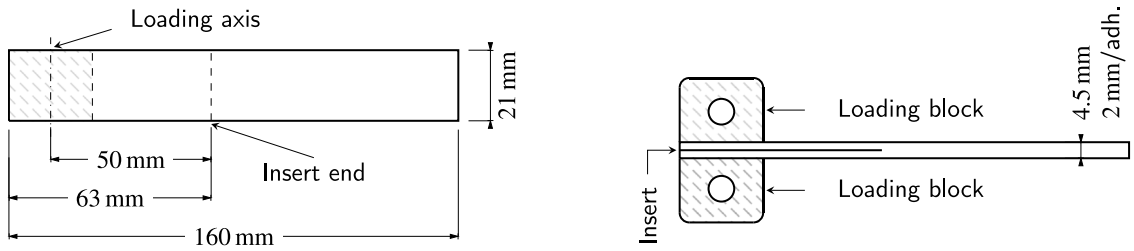

Fig. 6. DCB specimen design, fixtures and dimensions.

a joint finite Gaussian distribution. Therefore, a GP is fully defined via its mean function $\mu(x)$ and covariance function $k(x, x')$ [17]. A function $f(x)$ distributed as a GP can therefore be expressed as

$$f \sim \mathcal{N}(\mu(x), k). \tag{2}$$

The covariance is defined by a kernel function that in turn is a function of the distance between two points. As a result, for points close to each other the correlation between them is higher than for points far apart in the design space [32].

Given a set of training data points (X, f), where X_i is a 3-dimensional vector, and yet unobserved testing data points (X_*, f_*), a joint posterior distribution under the GP is then defined as

$$\begin{bmatrix} f \\ f_* \end{bmatrix} \sim \mathcal{N}\left(\begin{bmatrix} \mu_X \\ \mu_{X_*} \end{bmatrix}, \begin{bmatrix} K_{X,X} & K_{X,X_*} \\ K_{X_*,X} & K_{X_*,X_*} \end{bmatrix}\right) = \mathcal{N}\left(\begin{bmatrix} \mu_X \\ \mu_{X_*} \end{bmatrix}, \begin{bmatrix} K & K_* \\ K_*^T & K_{**} \end{bmatrix}\right). \tag{3}$$

In Eq. (3), K is the kernel matrix of the training data points, K_* is the training–testing data kernel matrix and K_{**} is the testing data kernel matrix. Each of the submatrices elements, e.g. $K_{i,j}$, is defined by the kernel function $k(x_i, x_j)$. For processing parameter combinations that lie far outside of the studied design space either joining is not possible or severe thermal degradation occurs. Therefore, resulting in a fracture toughness close or equal to 0. Thus a constant mean (μ_x) equal to 0 is assumed. Eq. (3) therefore can be simplified to

$$\begin{bmatrix} f \\ f_* \end{bmatrix} \sim \mathcal{N}\left(\begin{bmatrix} 0 \\ 0 \end{bmatrix}, \begin{bmatrix} K & K_* \\ K_*^T & K_{**} \end{bmatrix}\right). \tag{4}$$

For simplification, by assuming no noise the conditional distribution at any test point x_* is given by

$$f_* \mid (f_1, \ldots, f_n, x_1, \ldots, x_n, x_*) \sim \mathcal{N}\left(K_*^T K^{-1} f, K_{**} - K_*^T K^{-1} K_*\right). \tag{5}$$

Each element of the kernel matrices K, K_* and K_{**} is solely a function of X and the kernel's hyperparameters.

3.1. Kernel selection

Although any non-negative function may be used as a kernel function, it is crucial to define a kernel function suitable for the process investigated as it constrains the form of the target function [32]. For this study, the kernel function was chosen as the summation of a white kernel and the product of a constant kernel and a radial basis function kernel. The kernel function is given by

$$K_{i,j} = AK_{RBF} + K_{noise}, \tag{6}$$

where $A \in \mathbb{R}^+$ is a constant. The radial basis function kernel (K_{RBF}) is a smooth stationary kernel, defined as

$$K_{RBF} = exp\left(-\frac{\|x_i - x_j\|^2}{2l^2}\right), \tag{7}$$

where $l \in \mathbb{R}^+$ is a three-dimensional vector describing the length scale of the kernel and thus determines the smoothness. Although it is expected that the function needs to account for sudden changes in fracture toughness, a radial basis function was chosen as it would allow for minimising the number of trials required to explore the design space. For a larger number of samples, a Matérn kernel may be better suited to capture this behaviour [32]. The white kernel describes the noise associated with the signal as independent and identically normally distributed. In addition, an additional Gaussian noise is added during the fitting of the emulator. Both noise levels are added to the diagonal of the covariance matrix. The white noise kernel is given by

$$K_{noise} = \lambda, \text{ if } x_i \equiv x_j, \text{ else } 0. \tag{8}$$

Adding noise is necessary to account for the expected variance in both empirical training data and data associated with any test point within the design parameter space.

3.2. Initial training point selection

Ten initial training points were selected using maximin Latin hypercube sampling, therefore, aiming to maximise the minimum Euclidean distance between sampling points in the design space, as outlined in Table 1. The welding parameter combinations of the initial sampling points are shown in Table 2.

Table 2
Initial sampling points based on maximin Latin hypercube sampling.

Sample	Time [s]	Temperature [°C]	Pressure [MPa]
1	75	270	1.2
2	35	310	1.1
3	25	290	0.8
4	55	340	1.4
5	45	265	1.0
6	15	330	0.9
7	30	250	1.3
8	65	290	1.5
9	70	315	0.7
10	85	350	1.0

Results obtained were then used to train the GP emulator. Thus a first approximation of the kernel functions hyperparameters by minimising the log-marginal-likelihood was obtained.

3.3. Statistical model optimisation

Further learning of the underlying function of the GP emulator can be achieved by exploration of the parameter space, and via exploitation optimum values could be obtained. For this study, the main focus is to determine processing windows and thus explore the design space.

Given a set X_S containing several new sampling points, the aim is to select N distinct sampling points $X_T = [x_1^*, \ldots, x_n^*] \in X_S$, such that the mean average standard deviation ($\overline{\sigma}$) of the studied processing parameter space is minimised. To predict how adding N training points to the existing number of training points affects the standard deviation of the studied design space, it is assumed that all values f^* associated with X_t have been observed. Using the obtained hyperparameters based on the initial training data set and using Eq. (5) it can be seen that the new standard deviation can be recomputed. By recalculating $\overline{\sigma}$ for every

possible combination of N distinct sampling points within X_S it is possible to find the subset yielding the best improvement in parameter space exploration.

However, testing every possible combination of N new sampling points is very computationally expensive. Therefore, an exchange algorithm was implemented. The algorithm replaces $x_i^* \in X_T$ with every $x_s \in X_S$ and replaces x_i^* with x_s yielding the minimum possible $\overline{\sigma}$. This is repeated for x_{i+1}^* to x_n^*. If no further reduction of $\overline{\sigma}$ can be obtained the current subset $X_T \in X_S$ is the proposed set of N new sampling points. Once a suitable combination of new sampling points is determined, the real toughness values need to be evaluated and the GP emulator has to be retrained. Although the suggested new training points are chosen such that $\overline{\sigma}$ is minimised, it has to be noted that after obtaining the empirical values associated with X_T and retraining the GP emulator the hyperparameters are likely to change. Optimisation therefore has to be repeated until either exploration of the design space is satisfactory or no significant changes to the hyperparameters are observed.

For this study, statistical optimisation was performed once, whereby five additional training points were determined. Additional suggested sampling points based on the implemented optimisation algorithm are outlined in Table 3.

Table 3
Additional sampling points based on initial GP fit.

Sample	Time [s]	Temperature [°C]	Pressure [MPa]
11	75	290	1.0
12	70	320	1.2
13	35	270	1.2
14	30	340	1.0
15	25	320	1.4

4. Results

In this section empirical Mode I fracture toughness results for the 15 different welding parameter combinations, shown in Tables 2 and 3, are outlined. Examples of load vs. displacement curves and R-curves, showing the toughness vs. crack length, for high-performance and weak-performance joints are shown. Furthermore, the fracture surface and failure mechanism of insufficiently processed, adequately processed and overprocessed joints are demonstrated. Initiation fracture toughness values of the initial loading cycle (growing the crack from the front of the precrack insert) were then used to train the GP emulator. The statistical model is used to identify the correlation between different processing parameters and an optimum processing parameter window yielding high-performance joints.

4.1. Mode I fracture toughness - Double Cantilever Beam experiments

Results obtained from the initial experiments (samples 1–10) and the five additional DCB tests (samples 11–15) are shown in Table 4. All fracture toughness values presented are scaled and do not represent absolute values.

The Mode I fracture toughness for Cetex® TC1000 CF/PEI, as determined by Akkerman et al. [33] to be approximately 1080 J/m^2 was chosen as the reference fracture toughness value. Mode I toughness values were scaled, with respect to the reference G_{IC} value and the minimum observed G_{IC}. It can be seen from Table 4 that the choice of welding parameters has a significant impact on the Mode I fracture toughness of resistance-welded thermoset joints. For a range of parameter combinations, an initiation G_{IC} comparable to that of a CF/PEI laminate [33] was obtained. Initiation values presented are taken from the initial loading trials. This was chosen because post-initiation glass fibre bridging and metal mesh bridging were observed for most specimens, which increases the Mode I fracture toughness. However, this phenomenon prevents identification of the true G_{IC} and thus would make comparison between different samples more challenging. The onset of fibre bridging was observed to occur post crack initiation of the initial loading and thus the effect on the initiation G_{IC} for the reload cycle was strongly influenced by the degree of fibre bridging.

Table 4
Scaled G_{IC} data for all DCB specimens and CF/PEI reference.

Sample	Initiation G_{IC}	Propagation G_{IC}	Minimum G_{IC}
REF. CF/PEI [33]	1.00	–	–
1	1.20	2.51	1.20
2	1.30	2.49	1.30
3	0.93	1.43	0.93
4	0.00	0.11	0.00
5	1.10	2.51	1.10
6	1.16	3.08	1.16
7	1.13	2.25	1.13
8	1.03	1.97	1.03
9	0.71	2.50	0.71
10	0.24	0.32	0.24
11	1.20	2.31	1.20
12	0.85	1.68	0.85
13	0.84	2.77	0.84
14	0.94	2.22	0.94
15	0.23	0.54	0.23

4.1.1. High-performance welds

For high-performance joints, primarily stable crack propagation was observed. The main failure mode was interfacial failure between the GF/PEI insulation layer and the metal mesh. Post crack initiation, crack propagation tended towards the joints mid-plane. As a result, GF bridging was observed as the crack passed through the GF/PEI insulation layer. Resulting GF and metal mesh bridging led to a significant increase in the local fracture toughness and the joint's load-bearing capability. Further crack propagation occurred at the resin-rich region between the GF/PEI insulation and the metal mesh. The force vs. cross-head displacement and R-curve (G_{IC} vs. crack-extension) plots of sample 1 (example of a high-performance weld) are shown in Figs. 7(a) and 7(b) respectively. Figs. 7(c) and 7(d) show in-situ images of GF and mesh bridging and post GF breakage and mesh tearing at points (1) and (2) respectively.

Throughout crack propagation metal mesh bridging and glass fibre mesh bridging was observed at distinct crack-extensions thus resulting in a fluctuating fracture toughness. For samples that showed a high degree of fibre or metal mesh bridging, the resulting significant energy peak (reflected by a significant local fracture toughness increase) resulted in a sudden unstable crack growth over a distinct crack extension once fibre breakage or mesh tearing occurred.

4.1.2. Insufficiently processed and overprocessed welds

For insufficiently processed welds, the main failure mode is interfacial failure between the PEI coupling layer of the laminate and the GF/PEI insulation layer of the HE. This indicates a poor consolidation quality as a result of low processing temperatures and very short welding times and thus polymer diffusion is limited. Little to no glass fibre and metal mesh bridging was observed. Overprocessed welds showed a similar crack propagation behaviour to high-performance joints. Failure was driven by interfacial failure between the stainless steel mesh and the GF/PEI insulation and resin rupture.

Both insufficiently processed and overprocessed welds showed a reduced load-bearing capability and therefore lower fracture toughness values. For samples 4 and 10, which were both overprocessed, unstable crack propagation was observed, which is a result of the high degree of porosity present at the joint interface. A representative example of a force vs. cross-head displacement and R-curve plots for an overprocessed weld (sample 10) are shown in Figs. 8(a) and 8(b). In Fig. 8(a), a sudden load drop associated with a sudden large crack

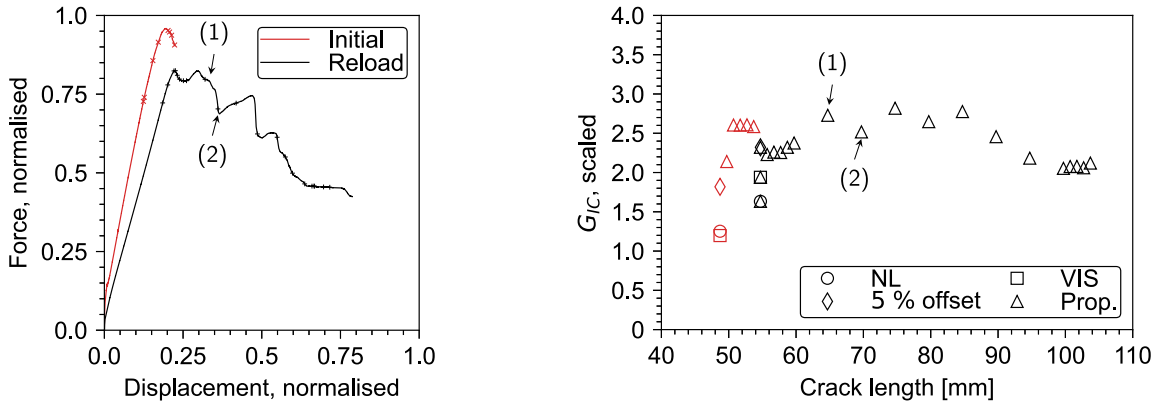

(a) Sample 1 force-displacement traces.

(b) Sample 1 R-curve.

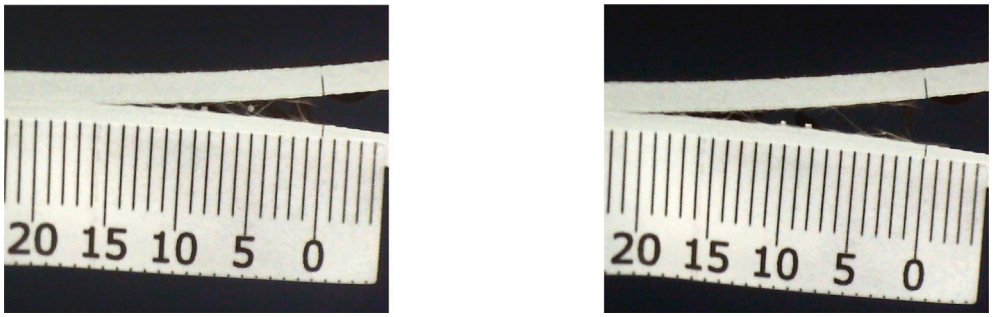

(c) Fibre and metal mesh bridging (1).

(d) Fibre breakage and mesh tearing (2).

Fig. 7. Force vs. displacement (a) and crack-resistance curve (R-curve) (b) plots for the initial and reload cycle of sample 1 (example of a high-performance weld). GF and steel mesh bridging (1) and failure (2) are shown in (c) and (d).

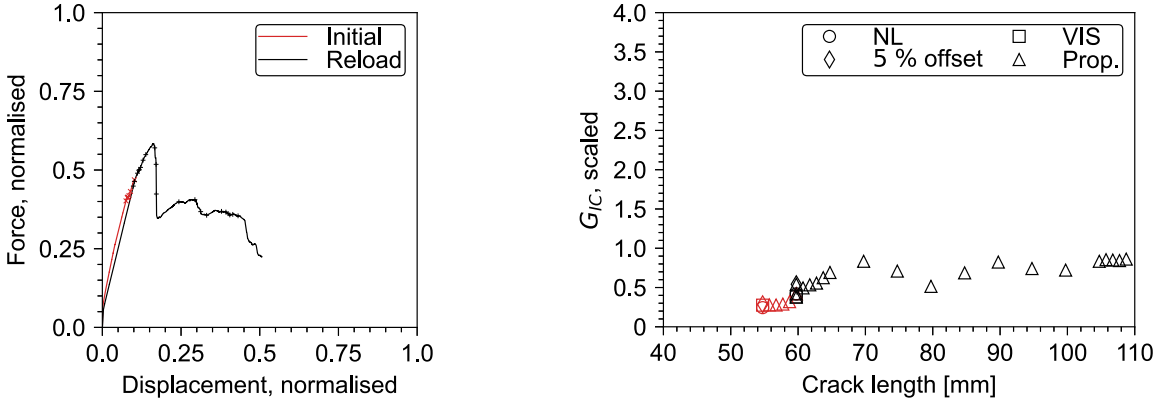

(a) Sample 10 force-displacement traces.

(b) Sample 10 R-curve.

Fig. 8. Force vs. displacement (a) and crack-resistance curve (R-curve) (b) plots for the initial and reload cycle of sample 10 (example of an overprocessed weld).

growth (approx. 15 mm) can be seen. Prior to fibre breakage, similar to a high-performance weld fibre bridging locally increases the fracture toughness as the bridged fibres increase the load-bearing capability.

4.2. Joint fractography

Optical microscopy of the fracture surface of DCB specimens allowed the identification of multiple failure modes. These include (i) tearing of the stainless steel mesh, (ii) glass fibre breakage, (iii) interfacial failure between the GF/PEI layer and the coupling layer, (iv) PEI resin rupture and (v) interfacial failure between the GF/PEI layer and the stainless steel mesh.

4.2.1. High-performance welds

The top and bottom fracture surfaces of a high-performance weld (sample 1) are shown in Figs. 9(a) and 9(b). It can be seen in Fig. 9(a), glass fibre bridging occurred post crack initiation as the crack propagates towards the joint mid-plane, followed by fibre breakage. Further crack propagation was primarily driven by interfacial failure between the GF/PEI layer and the metal mesh. Additionally, PEI matrix cracking and fibre breakage and metal mesh tearing were observed. The fracture surface shows a good level of interdiffusion of the PEI matrix within the gaps of the stainless steel mesh. Furthermore, no visible sign of thermal degradation can be observed. Fig. 9(c) shows metal mesh tearing at a distinct crack extension.

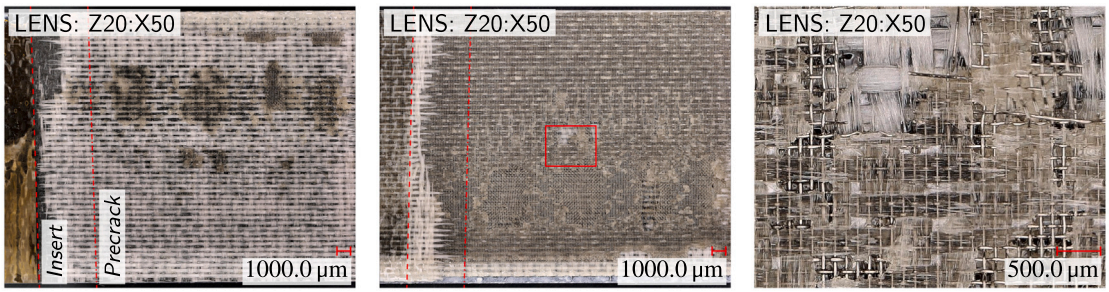

Fig. 9. Optical microscopy of the fracture surfaces of sample 1 (example of a high-performance weld). The insert crack front and precracked crack front post initial loading are shown in (a) and (b). A magnified view is shown in (c).

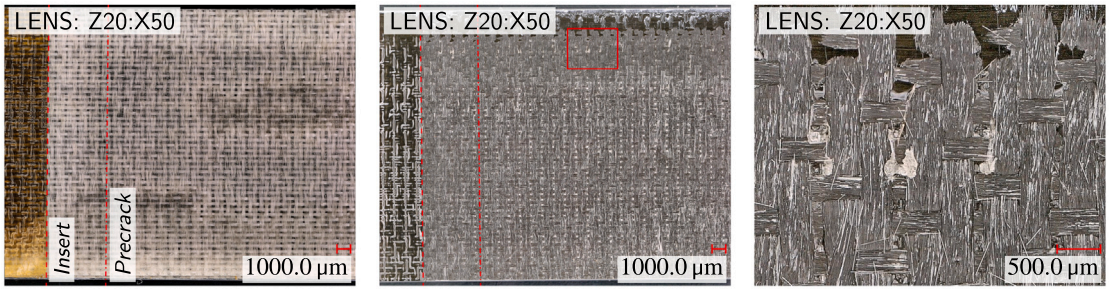

Fig. 10. Optical microscopy of the fracture surfaces of sample 7 (example of an insufficiently processed weld). The insert crack front and precracked crack front post initial loading are shown in (a) and (b). A magnified view is shown in (c).

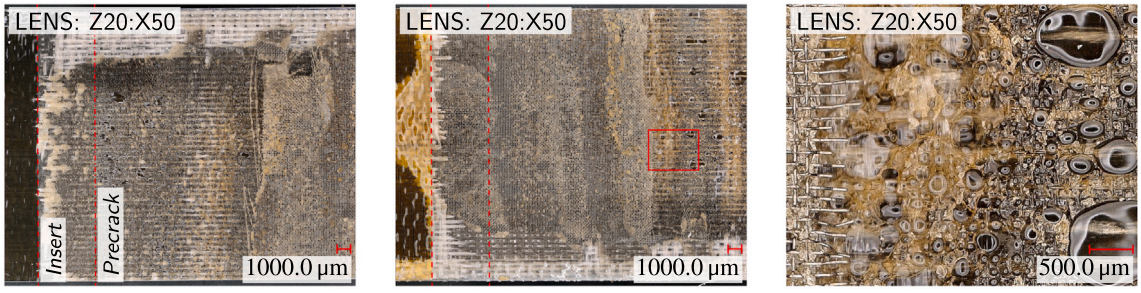

Fig. 11. Optical microscopy of the fracture surfaces of sample 10 (example of an overprocessed weld). The insert crack front and precracked crack front post initial loading are shown in (a) and (b). A magnified view is shown in (c).

4.2.2. *Insufficiently processed welds*

The main failure mode for insufficiently processed welds is interfacial failure between the GF/PEI layer and the thermoset laminate. No fibre bridging or metal mesh tearing occurred. As an example of an insufficiently processed weld, the fracture surfaces of sample 7 are shown in Fig. 10. Fig. 10(c), shows imprints of the glass fibres within the coupling layer and small unwelded patches close to the coupon edge. This indicates poor polymer interdiffusion due to too short welding times or low temperatures combined with low pressures. Insufficiently processed welds show reduced mode I fracture toughness performance, as shown for sample 7 in Table 4. However, insufficiently processed welds can be reprocessed.

4.2.3. *Overprocessed welds*

Overprocessed welds are defined as welds that showcase signs of thermal degradation. It was observed that interfacial failure between the GF/PEI layers and the metal mesh combined with cohesive failure of the PEI matrix were the main failure modes. As a result of thermal degradation the fracture surface shows resin discoloration and a high degree of porosity can be observed. Porosity, trapped inside the consolidated PEI pool post-welding is attributed to partial sublimation of the thermoset matrix. This phenomenon was previously observed by Villegas et al. [10] on ultrasonic-welded hybrid thermoplastic thermoset composite joints. As shown in Fig. 8, the mechanical performance of overprocessed welds is significantly reduced. Fracture surfaces of both sides of an overprocessed weld (sample 10) are shown in Figs. 11(a) and 11(b). Fig. 11(c) shows a magnified view of the fracture surface.

4.3. *Gaussian process emulator*

For damage tolerant design, commonly the initiation or minimum G_{IC} values are used [28]. These empirical values (X, f) were used to train a 3-dimensional multivariate GP emulator, as described in Section 3. Using the GP emulator the variation of G_{IC} across the design space and its associated standard deviation $(\overline{\sigma})$ were predicted.

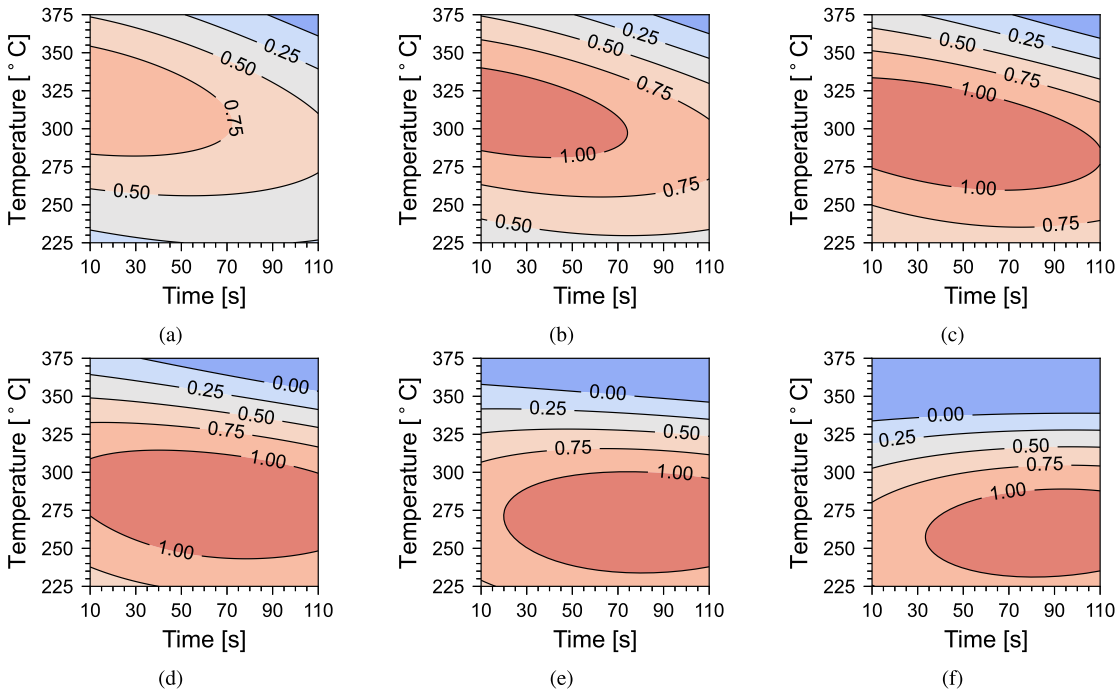

Fig. 12. Posterior prediction surfaces at constant pressures (a) 0.70 MPa, (b) 0.85 MPa, (c) 1.00 MPa, (d) 1.15 MPa, (e) 1.30 MPa and (f) 1.45 MPa.

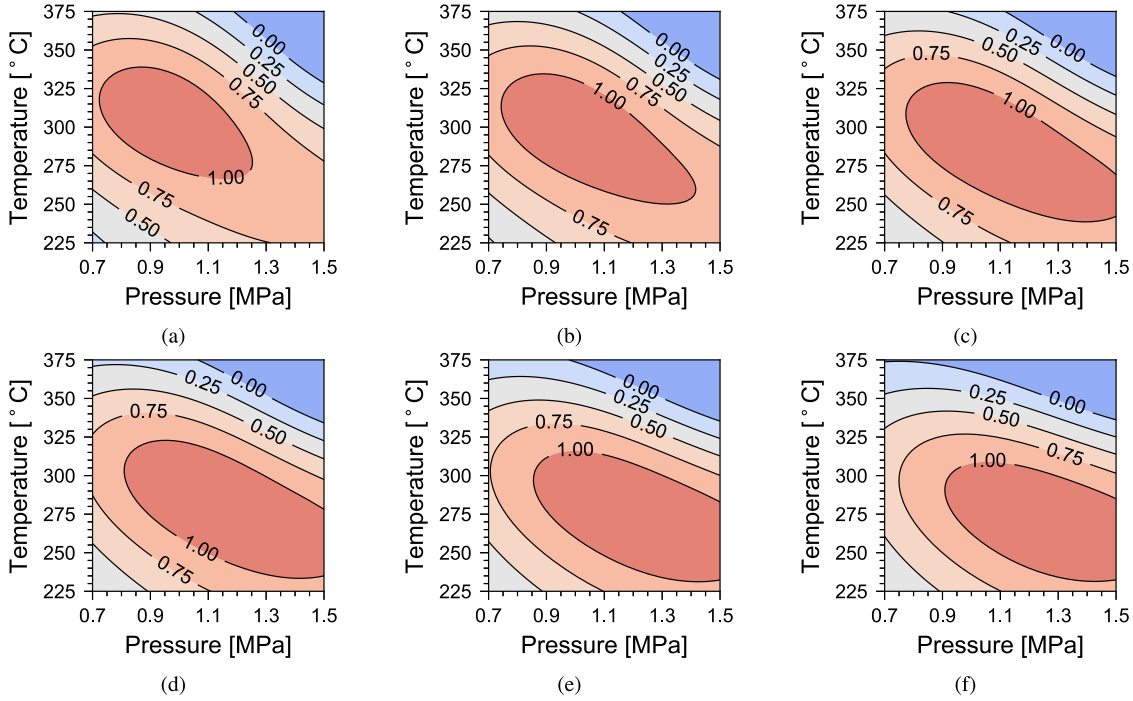

Fig. 13. Posterior prediction surfaces at constant welding times (a) 15 s, (b) 30 s, (c) 45 s, (d) 60 s, (e) 75 s and (f) 90 s.

The effect of processing parameters on the joint's performance is illustrated via contour surfaces, whereby one parameter is kept constant and the Mode I fracture toughness is represented as a function of two key processing parameters. Fig. 12 shows G_{IC} as a function of temperature and time (at target welding temperature) at increasing constant pressure slices.

Similarly, Figs. 13(a) to 13(f) show the variation of G_{IC} as a function of temperature and pressure at increasing constant processing times.

The posterior predictions of the GP emulator in Figs. 12 and 13 reveal that for a considerable range of welding parameter combinations, a mechanical performance close to the baseline CF/PEI reference is achievable. To manufacture a high-performance joint, a sufficiently high welding pressure was found to be key. Pressures greater than 0.75 MPa were required to remove trapped air at the interface and promote polymer interdiffusion. However, it is also seen in Figs. 12 and 13 that with increasing pressure lower welding temperatures are required.

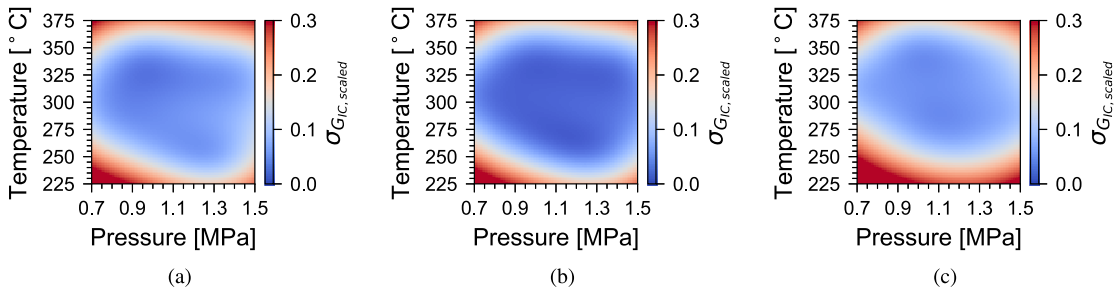

Fig. 14. GP emulator variation of standard deviation as a function of temperature and pressure at constant welding times (a) 15 s, (b) 45 s and (c) 90 s.

Furthermore, it was observed that higher temperatures require shorter welding times and lower temperatures require longer welding times.

The predicted G_{IC} values of the lower bound 95% confidence interval were used to determine recommended processing parameter ranges. The recommended parameter ranges yielding a Mode I fracture toughness performance comparable to the reference CF/PEI laminate are shown in Table 5.

Table 5
Recommended welding parameter ranges yielding high-performance joints.

Parameter	Minimum	Maximum
Temperature [°C]	300	325
Time [s]	25	50
Pressure [MPa]	0.85	1.05

Another advantage of using a Bayesian approach to study the influence and correlation of key welding parameters is the capability to extract uncertainty measurements of the fracture toughness predictions. As only one sample was tested per parameter configuration it is assumed that G_{IC} values at each training point are noisy. Thus a Gaussian noise with a variance of 0.1 was applied. The scaled mean standard deviation ($\overline{\sigma}$) and maximum standard deviation (σ_{max}) across the studied parameter space are 0.05 and 0.30 respectively. It has to be noted that although the maximum standard deviation is rather high, it is associated with test points (x^*) at the boundary of the studied parameter space. As no samples used manufacturing parameters at the limits of the studied design space it is expected that the uncertainty prediction of the GP emulator significantly increases in this unexplored region. Fig. 14 illustrates the scaled standard deviation as a function of temperature and pressure at increasing constant processing times.

5. Discussion

For a range of different key welding parameter combinations an initiation Mode I fracture toughness (G_{IC}) comparable to the chosen reference G_{IC} of approximately 1080 J/m^2 for CF/PEI [33] was achieved. The interlaminar fracture toughness for the thermoset laminate used in this study (HexPly®IM7/8552) is approximately 277 J/m^2 [34]. Comparing this with the performance observed for resistance-welded joints a significant Mode I fracture toughness improvement of approximately 290% vs. a thermoset bonded joint was obtained. Additionally, compared to thermoset bonding using a standard autoclave cycle, the welding cycle times are up to 98% shorter and the need for complex surface preparation is practically eliminated.

5.1. Fracture behaviour

The crack propagation was observed along the joint interface and did not propagate into the thermoset laminate for all but sample 3. For sample 3, the crack propagated into the thermoset laminate after a crack growth of approximately 25 mm. This was most likely due to unsymmetric load introduction by the loading blocks, as there was no indication of thermal degradation. This lack of symmetry in the load application further emphasises the challenges faced by commonly used single-lap shear testing [15]. This challenge makes it difficult to obtain representative empirical data to assess and compare the joint's performance. However, although a comparison of the effects of differing processing parameters is not possible once the crack has propagated into the thermoset laminate, it does indicate that the performance of the joint is better than the interlaminar toughness of the thermoset laminate. Hence, it demonstrates that the joint may not be the weakest part of a structure.

Except for specimens with insufficiently processed welds, all tested specimens showed some fibre-bridging over distinct crack extension regions. It was observed that fibre-bridging can significantly increase the local fracture toughness. Though, the exact location where this phenomenon occurred varied and thus, it can prove difficult to obtain representative fracture toughness values, especially if fibre bridging happens at or immediately after crack initiation. A potential reason favouring fibre-bridging just after the onset of crack growth is the initial small offset of the precrack insert from the joints mid-plane. Further crack propagation tended towards the mid-plane where the metal mesh was placed and thus favouring metal mesh bridging. Both insufficient- and overprocessing, results in weak joints, whereby sudden run arrest crack extensions are likely. Insufficiently processed joints are prone to fail due to poor interdiffusion between the different thermoplastic resin layers and the crack extension is most likely to occur at the interface farthest away from the heat source between the PEI coupling layer and the GF/PEI layers. These joints however may be reprocessed. Overprocessed welds result in thermal degradation of the thermoset matrix which in turn makes the welded components unusable.

5.2. Processing parameter windows using a Gaussian process emulator

This study demonstrates that statistical methods, outlined in Section 3, can be successfully used to minimise the number of sampling points required to estimate the performance of a joint subject to different key manufacturing processing parameters. Using the GP emulator's posterior prediction, correlations between the studied three main processing parameters, (i) temperature, (ii) time and (iii) pressure can be identified. In addition, it is possible to determine processing parameter ranges yielding high-performance joints. Overall with just 15 different sampling points (X) a satisfactory exploration of the design space was achieved. However, boundary regions of the design space are less explored thus having a significantly higher standard deviation. As the aim of this study was the exploration of the parameter space, optimum processing parameters cannot readily be identified using the current training data set (X, f) and further sampling and statistical model optimisation would be required to obtain these. Optimum processing parameters, however, may be difficult to obtain even with further optimisation, as the onset of fibre bridging cannot be predicted and may result in misleading and potentially overly optimistic G_{IC} values and in addition to the key processing parameters several secondary parameters that were not investigated in this study influence the performance of a welded joint.

Furthermore, with an increasing number of sampling points a more accurate posterior prediction would be possible allowing to further optimise the hyperparameters of the kernel function. In addition, further improvement of the accuracy of the posterior prediction and alteration of the Gaussian noise applied to the initial training points would be possible by increasing the number of samples for each training point. However, this is outside the scope of this study as the aim was to demonstrate that high-performance joints, having a significantly higher Mode I fracture toughness than thermoset composites, can be manufactured and processing windows can be determined using statistical methods such as Gaussian processes.

5.3. Processing parameters yielding high performance

Predicted welding parameter correlations have shown that short cycle times require higher temperatures and lower pressures can be used. For low temperature welding, heat has to be applied for longer and higher pressures are favoured. Excessive pressures may yield increased amounts of resin being squeezed out of the joint interface and could damage the laminate [6]. High transverse pressures were found to lead to shear band formation due to plastic deformation of the matrix leading to interface decohesion [35]. The correlation between processing parameters is believed to be related to the ability of individual PEI layers to diffuse and thus to the viscosity during the welding process. It was observed by Tsiangou et al. [5] that the viscosity of PEI starts to reduce linearly above 250 °C from around 200 kNs/m^2 to 2 kNs/m^2 at 350 °C. Viscosity directly affects how well polymers can interdiffuse, with lower viscosity allowing for faster diffusion [4,36]. Therefore, to counterbalance the reduced ability to diffuse at low processing temperatures, higher pressures and longer welding cycles are required.

Optimum processing parameters are therefore a trade-off between ensuring good interdiffusion at the joint interface and preventing thermal degradation of the thermoset matrix. Abouhamzeh et al. [27] have found that for the used thermoset laminate (HexPly®IM7/8552) thermal degradation initiates at around 242 °C. Thus lower processing temperatures are favourable, however, as processing temperatures in excess of 250 °C are needed, long welding times might result in thermal degradation regardless. The risk of thermal degradation can be limited by, for example, increasing the thickness of the PEI coupling layer [5]. This study has shown that using heatsinks as a means of passive cooling of the external surfaces of the thermoset laminate during the welding process is beneficial.

Furthermore, previous studies, for example, by Ageorges et al. [36] and Zweifel et al. [12] used constant power welding to study the influence of processing parameters on joint performance. However, it was observed that the required power is highly dependent on numerous factors including, (i) geometry and temperature of the heatsinks, (ii) interface temperature, as with increasing temperature the resistance of the stainless steel mesh reduces and (iii) the type and size of the conductor. Thus the novel approach of varying power levels during the welding process allows to more precisely control the heat-up and cool-down rate and maintain a constant interface temperature. Therefore, the process is more easily repeatable, the influence of processing parameters on joint performance is more readily comparable and the risk of thermal degradation is more controllable. Amongst other factors, non-destructive inspection methods that allow to identify the quality of adhesion are not available today. Therefore, the certification of thermoset bonded joints for primary aerospace structures is limited [9]. In contrast to adhesive bonding the joint performance does not rely on the quality of surface preparation but rather the chemical compatibility between the different polymers used. This could aid the certification process in the near future.

6. Conclusion

It is demonstrated that resistance welding is a very promising novel method for joining aerospace-grade thermoset composite components. The obtained Mode I fracture toughness is comparable to high-performance aerospace-grade thermoplastic composites. When compared to a co-cured thermoset composite joint a significant performance improvement of approximately 290% is feasible. A novel adaptive welding method based on in-situ process monitoring of the joint interface was used, enabling improved process control and ensuring process repeatability.

Using a Gaussian process emulator the joint's performance dependency on the three key welding parameters, temperature, time and pressure was studied and the correlations between them were identified. Furthermore, the emulator was used to define processing windows yielding high-performance joints. Results showed that a wide range of parameter combinations produce welds with similarly high fracture toughness to high-performance thermoplastic composites. It was observed that higher temperatures require shorter welding times, with lower pressures improving the performance, whereas for low temperatures, high pressures are desirable and longer processing times can be used. The selection of adequate processing parameters is key for avoiding detrimental thermal degradation of the thermoset matrix whilst ensuring a fully processed joint. Fractography of the joints was used to identify the effects of different welding parameters on the joint's failure mechanism.

Future work will focus on rigorous testing of individual welding parameters to demonstrate the robustness and repeatability of the process. Additional test methods to examine further joint properties will also be applied.

CRediT authorship contribution statement

Thomas Maierhofer: Conceptualization, Methodology, Investigation, Formal analysis, Welding rig design & construction, Software - Welding process control & monitoring, Software - Gaussian process emulator, Visualization, Writing – original draft. **Evripides G. Loukaides:** Conceptualization, Supervision, Writing – review & editing. **Craig Carr:** Conceptualization, Writing – review & editing. **Chiara Bisagni:** Conceptualization, Supervision, Writing – review & editing. **Richard Butler:** Conceptualization, Supervision, Methodology, Writing – review & editing.

Declaration of competing interest

The authors declare that they have no known competing financial interests or personal relationships that could have appeared to influence the work reported in this paper.

Data availability

The data that has been used is confidential.

Acknowledgements

The authors gratefully acknowledge the continuous project support and industrial guidance by GKN Aerospace UK. This research project was supported by the EPSRC, UK, Programme Grant: "Certification for Design: Reshaping the Testing Pyramid" (CerTest, EP/S017038/1). The authors would also like to thank Carl Scarth and Evangelos Evangelou (both University of Bath) for their support and advice on Gaussian processes.

References

[1] Brauner C, Nakouzi S, Zweifel L, Tresch J. Co-curing behaviour of thermoset composites with a thermoplastic boundary layer for welding purposes. Adv Compos Lett 2020;29:1–9. http://dx.doi.org/10.1177/2633366X20902777.

[2] Xiong X, Wang D, Wei J, Zhao P, Ren R, Dong J, Cui X. Resistance welding technology of fiber reinforced polymer composites: a review. J Adhes Sci Technol 2021;35(15):1593–619. http://dx.doi.org/10.1080/01694243.2020.1856514.

[3] Curran R, Kundu AK, Wright JM, Crosby S, Price M, Raghunathan S, Benard E. Modelling of aircraft manufacturing cost at the concept stage. Int J Adv Manuf Technol 2006;31(3–4):407–20. http://dx.doi.org/10.1007/s00170-005-0205-8.

[4] Deng S, Djukic L, Paton R, Ye L. Thermoplastic-epoxy interactions and their potential applications in joining composite structures - A review. Composites A 2015;68:121–32. http://dx.doi.org/10.1016/j.compositesa.2014.09.027.

[5] Tsiangou E, Teixeira de Freitas S, Fernandez Villegas I, Benedictus R. Ultrasonic welding of epoxy- to polyetheretherketone- based composites: Investigation on the material of the energy director and the thickness of the coupling layer. J Compos Mater 2020;54(22):3081–98. http://dx.doi.org/10.1177/0021998320910207.

[6] Xie L, Liu H, Wu W, Abliz D, Duan Y, Li D. Fusion bonding of thermosets composite structures with thermoplastic binder co-cure and prepreg interlayer in electrical resistance welding. Mater Des 2016;98:143–9. http://dx.doi.org/10.1016/j.matdes.2016.03.020.

[7] Lionetto F, Morillas MN, Pappadà S, Buccoliero G, Fernandez Villegas I, Maffezzoli A. Hybrid welding of carbon-fiber reinforced epoxy based composites. Composites A 2018;104:32–40. http://dx.doi.org/10.1016/j.compositesa.2017.10.021.

[8] Ageorges C, Ye L, Hou M. Advances in fusion bonding techniques for joining thermoplastic matrix composites: a review. Compos - A: Appl Sci Manuf 2001;32(6):839–57. http://dx.doi.org/10.1016/S1359-835X(00)00166-4.

[9] Löbel T, Holzhüter D, Sinapius M, Hühne C. A hybrid bondline concept for bonded composite joints. Int J Adhes Adhes 2016;68:229–38. http://dx.doi.org/10.1016/j.ijadhadh.2016.03.025.

[10] Fernandez Villegas I, Vizcaino Rubio P. On avoiding thermal degradation during welding of high-performance thermoplastic composites to thermoset composites. Composites A 2015;77:172–80. http://dx.doi.org/10.1016/j.compositesa.2015.07.002.

[11] Tijs BHAH, Doldersum MHJ, Turon A, Waleson JEA, Bisagni C. Experimental and numerical evaluation of conduction welded thermoplastic composite joints. Compos Struct 2022;281:114964. http://dx.doi.org/10.1016/j.compstruct.2021.114964.

[12] Zweifel L, Brunner J, Nakouzi-Queloz S, Brauner C, Dransfeld C. Development of a resistance welding process for thermoset fiber composite components with co-cured thermoplastic boundary layer. In: Proceedings of the 18th European conference on composite materials (ECCM18). Athens, Greece: University of Patras, Laboratory of Applied Mechanics and Vibrations; 2018.

[13] Bauer S, Endraß M, Doll G, Jarka S, Thellmann A, Schuster A. Mechanical Investigation of resistance welded high-performance reinforced thermoplastics. In: Proceedings of the 4th international conference & exhibition on thermoplastic composites (ITHEC 2018). (Manuscript P07):Bremen, Germany: Messe Bremen; 2018, p. 1–4.

[14] Ageorges C, Ye L, Hou M. Experimental investigation of the resistance welding for thermoplastic-matrix composites. Part I: Heating element and heat transfer. Compos Sci Technol 2000;60(7):1027–39. http://dx.doi.org/10.1016/S0266-3538(00)00005-1.

[15] Redmann A, Damodaran V, Tischer F, Prabhakar P, Osswald TA. Evaluation of Single-Lap and Block Shear Test Methods in Adhesively Bonded Composite Joints. J Compos Sci 2021;5(1):27. http://dx.doi.org/10.3390/jcs5010027.

[16] Siddique A, Abid S, Shafiq F, Nawab Y, Wang H, Shi B, Saleemi S, Sun B. Mode I fracture toughness of fiber-reinforced polymer composites: A review. J Ind Text 2021;50(8):1165–92. http://dx.doi.org/10.1177/1528083719858767, arXiv:https://doi.org/10.1177/1528083719858767.

[17] Rasmussen CE, Williams CKI. Gaussian processes for machine learning. Cambridge, MA: the MIT Press; 2006.

[18] Roychowdhury S, J. W. Gillespie J, Advani SG. Volatile-induced void formation in amorphous thermoplastic polymeric materials: I. Modeling and parametric studies. J Compos Mater 2001;35(4):340–66. http://dx.doi.org/10.1177/002199801772662208.

[19] Fernandez Villegas I, van Moorleghem R. Ultrasonic welding of carbon/epoxy and carbon/PEEK composites through a PEI thermoplastic coupling layer. Composites A 2018;109:75–83. http://dx.doi.org/10.1016/j.compositesa.2018.02.022, URL https://www.sciencedirect.com/science/article/pii/S1359835X18300630.

[20] Zweifel L, Brauner C, Teuwen J, Dransfeld C. In situ characterization of the reaction-diffusion behavior during the gradient interphase formation of polyetherimide with a high-temperature epoxy system. Polymers 2022;14(3). http://dx.doi.org/10.3390/polym14030435, URL https://www.mdpi.com/2073-4360/14/3/435.

[21] Hou M, Ye L, Mai Y-W. An Experimental Study of Resistance Welding of Carbon Fibre Fabric Reinforced Polyetherimide (CF Fabric/PEI) Composite Material. Adv Compos Mater 1999;6:35–49. http://dx.doi.org/10.1023/A:1008879402267.

[22] Dubé M, Hubert P, Gallet JNAH, Stavrov D, Bersee HEN, Yousefpour A. Metal mesh heating element size effect in resistance welding of thermoplastic composites. J Compos Mater 2012;46(8):911–9. http://dx.doi.org/10.1177/0021998311412986.

[23] Dubé M, Hubert P, Yousefpour A, Denault J. Current leakage prevention in resistance welding of carbon fibre reinforced thermoplastics. Compos Sci Technol 2008;68(6):1579–87. http://dx.doi.org/10.1016/j.compscitech.2007.09.008, URL https://www.sciencedirect.com/science/article/pii/S0266353807003600.

[24] Stavrov D, Bersee H. Resistance welding of thermoplastic composites-an overview. Composites A 2005;36(1):39–54. http://dx.doi.org/10.1016/j.compositesa.2004.06.030.

[25] Stavrov D, Beukers A, Bersee H. Experimental investigation of large-scale welding of carbon fiber thermoplastic composite materials. In: Proceedings of the 14th international conference on composite materials (ICCM14). (ID-1552):San Diego, CA, USA: Society of Manufacturing Engineers; 2003, p. 1–8.

[26] Don RC, Gillespie Jr. JW, Lambing CLT. Experimental characterization of processing-performance relationships of resistance welded graphite/polyetheretherketone composite joints. Polym Eng Sci 1992;32(9):620–31. http://dx.doi.org/10.1002/pen.760320908, arXiv:https://4spepublications.onlinelibrary.wiley.com/doi/pdf/10.1002/pen.760320908 URL https://4spepublications.onlinelibrary.wiley.com/doi/abs/10.1002/pen.760320908.

[27] Abouhamzeh M, Sinke J. Effects of fusion bonding on the thermoset composite. Composites A 2019;118:142–9. http://dx.doi.org/10.1016/j.compositesa.2018.12.031.

[28] ASTM International. Standard test method for mode I interlaminar fracture toughness of unidirectional fiber-reinforced polymer matrix composites. Standard ASTM D5528-13, West Conshohocken, PA: ASTM International; 2021, URL https://www.astm.org/d5528_d5528m-21.html.

[29] Renart J, Blanco N, Pajares E, Costa J, Lazcano S, Santacruz G. Side clamped beam (SCB) hinge system for delamination tests in beam-type composite specimens. Compos Sci Technol 2011;71(8):1023–9. http://dx.doi.org/10.1016/j.compscitech.2010.10.005, URL https://www.sciencedirect.com/science/article/pii/S026635381000388X.

[30] Maierhofer T, Loukaides EG, Hernandez T, Carr C, Bisagni C, Butler R. Fracture toughness and performance of resistance-welded and co-bonded thermoset/thermoplastic polymer composite hybrid joints. In: Vassilopoulos A, Michaud V, editors. Proceedings of the 20th European conference on composite materials (ECCM20). vol. 2, (Paper 61825):Laussane, Switzerland: EPFL Lausanne, Composite Construction Laboratory; 2022, p. 740–7. http://dx.doi.org/10.5075/epfl-298799_978-2-9701614-0-0.

[31] Gonçalves Araújo I, Santos LFP, Marques LFB, Reis JF, de Souza SDB, Botelho EC. Influence of environmental effect on thermal and mechanical properties of welded PPS/carbon fiber laminates. Mater Res Express 2019;6(10):105337. http://dx.doi.org/10.1088/2053-1591/ab3acd, URL https://iopscience.iop.org/article/10.1088/2053-1591/ab3acd.

[32] Chang J, Kim J, Zhang B-T, Pitt MA, Myung JI. Data-driven experimental design and model development using Gaussian process with active learning. Cogn Psychol 2021;125:101360. http://dx.doi.org/10.1016/S1566-1369(00)80003-5.

[33] Akkerman R, Reed PE, Huang KY, Warnet L. Comparison of fracture toughness (G_{IC}) values of polyetherimide (PEI) and a carbon-fibre/PEI composite: an experimental and theoretical study. Eur Struct Integr Soc 2000;27:3–14. http://dx.doi.org/10.1016/S1566-1369(00)80003-5.

[34] Camanho PP, Dávila PMCG. Prediction of size effects in notched laminates using continuum damage mechanics. Compos Sci Technol 2007;67(13):2715–27. http://dx.doi.org/10.1016/j.compscitech.2007.02.005, URL https://www.sciencedirect.com/science/article/pii/S0266353807000796.

[35] González C, LLorca J. Mechanical behavior of unidirectional fiber-reinforced polymers under transverse compression: Microscopic mechanisms and modeling. Compos Sci Technol 2007;67(13):2795–806. http://dx.doi.org/10.1016/j.compscitech.2007.02.001, URL https://www.sciencedirect.com/science/article/pii/S0266353807000711.

[36] Ageorges C, Ye L. Resistance welding of thermosetting composite/thermoplastic composite joints. Composites A 2001;32(11):1603–12. http://dx.doi.org/10.1016/S1359-835X(00)00183-4, URL https://www.sciencedirect.com/science/article/pii/S1359835X00001834.